Heliyon 10 (2024) e39618

Contents lists available at ScienceDirect

Heliyon

journal homepage: www.cell.com/heliyon

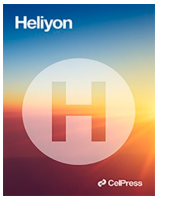

Research article

Thermoelectric properties of superionic $Li_{0.11}Cu_{1.89}S$ compound

Marzhan Kubenova [a,*], Malik Balapanov [b,**], Kairat Kuterbekov [a], Rais Ishembetov [b], Rafail Almukhametov [b], Kenzhebatyr Bekmyrza [a], Bulat Akhmetgaliev [b], Talgat Sharipov [b], Marat Zeleev [c], Asset Kabyshev [a], Zhamal Mukhanova [a], Bakhytkul Baikhozhaeva [a], Robert Yakshibaev [b]

[a] L.N. Gumilev Eurasian National University, Astana, Kazakhstan
[b] Ufa University of Science and Technology, Ufa, Russia
[c] Bashkir State Medical University, Ufa, Russia

ARTICLE INFO

Keywords:
Copper sulfide
Superionic conductor
Thermal conductivity
Seebeck coefficient
Electronic conductivity

ABSTRACT

Copper sulfide is a multifunctional material. Copper sulfides are known to be used in photoelectric converters, in plasmonics, in active electrodes of batteries and supercapacitors, etc. The excellent thermoelectric properties of copper sulfide are well-known too. The purpose of this study is to investigate the thermoelectric performance of nanocomposite copper sulfide contained monoclinic Cu_2S and tetragonal $Cu_{1.96}S$ phase. According to scanning electron microscopy, the average particle size of the synthesized powder was about 373 nm. The $Li_{0.11}Cu_{1.89}S$ sample showed an electronic conductivity of 50–180 S/cm, a Seebeck coefficient of 0.04–0.31 mV/K in the range of 300–700 K, and high power factor 5.8 μW $K^{-2}cm^{-1}$ at 672 K. Total thermal conductivity decreases with increasing temperature from 0.61 to 0.22 W•$K^{-1}m^{-1}$ in the range of 300–700 K. Such low thermal conductivity and high power factor made it possible to achieve an extremely high dimensionless thermoelectric figure of merit ZT = 1.76 at 672 K, which allows to consider the $Li_{0.11}Cu_{1.89}S$ alloy as a promising thermoelectric material.

1. Introduction

Copper sulfides and their alloys with alkali metals are known as promising superionic semiconductor materials [1–11]. They are phases of variable composition and have a wide range of homogeneity over the cationic sublattice, which makes it possible to control their useful properties by changing the degree of nonstoichiometry. The electronic conductivity of copper sulfide is due to holes arising from the ionization of nonstoichiometric vacancies in the copper sublattice; therefore, the value of the electronic conductivity σ_e strongly depends on the nonstoichiometry of the composition δ. According to Okamoto et al. [4], the $Cu_{2-\delta}S$ conductivity increases from 0.07 to 2400 S cm^{-1} with increasing deviation from the stoichiometric composition from $\delta = 0$ to $\delta = 0.2$. In the low-temperature phase, Sorokin et al. [2] observed impurity-type semiconductor conductivity with an activation energy of 0.09 eV and high mobility up to 1070 cm^2 V^{-1} s^{-1}; in the high-temperature phase above 693 K they discovered intrinsic conductivity with a band gap 1.8 ± 0.1 eV. According to O. Astakhov and V. Lobankov [3], intrinsic conductivity in copper sulfide occurs at 723–773 K; the band gap, determined from the temperature dependence of conductivity, at temperatures above 773 K is 1.4 eV. The optical band gap of the low-temperature

* Corresponding author.
** Corresponding author.
E-mail addresses: kubenova.m@yandex.kz (M. Kubenova), balapanovmk@mail.ru (M. Balapanov).

https://doi.org/10.1016/j.heliyon.2024.e39618
Received 7 August 2024; Received in revised form 18 October 2024; Accepted 18 October 2024
Available online 19 October 2024

Cu_2S phase is 1.21 eV at 300 K and 1.26 eV at 80 K [6], the authors point to an indirect optical transition.

Near stoichiometric copper(I) sulfide exists in three phases (γ, β, α). According to Ref. [12], copper sulfide at room temperature is usually a mixture of chalcocite Cu_2S and jurleite $Cu_{1.97}S$, which are in dynamic equilibrium with each other. Low-temperature chalcocite γ-Cu_2S has a monoclinic structure with the space group $P2_1/c$, passing at 376.5 K to the hexagonal phase β-Cu_2S with the space group P63/mmc [12]. Above 708 K, hexagonal chalcocite β-Cu_2S undergoes a transition to the cubic α-phase with the space group Fm3m [13]. Jurleite ($Cu_{1.965}S \div Cu_{1.934}S$) has a monoclinic lattice (space group P21/n) and is stable up to 366 ± 2 K [12], then reversibly decomposes into hexagonal chalcocite $Cu_{1.988}S$ and hexagonal digenite $Cu_{1.84}S$ [14]. In addition to these two phases, a metastable tetragonal phase Cu_2S is also found. According to Roseboom [14], the tetragonal phase occurs when copper sulfide (jurleite), heated to 110–350 °C, is cooled to 20 °C. The tetragonal phase also occurs under pressure, even when ground in a mortar or mill. The tetragonal phase may form a solid solution from at least $Cu_{1.96}S$ to Cu_2S. Skinner et al. [15] found the tetragonal phase at high pressures with the composition Cu_2S, and Janosi [16] obtained it with the composition $Cu_{1.96}S$. Roseboom [14] reports that the tetragonal phase can exist for several years, even after annealing at 500 °C.

The high temperature hexagonal and cubic copper sulfide phases are superionic and exhibit extremely high ionic conductivities and chemical diffusion coefficients [4,7]. Unique "liquid like" nature of copper sulfide and copper selenide causes colossal Seebeck coefficients in the narrow temperature interval where the low-temperature and the high temperature phases coexist in the chalcogenide specimen simultaneously [17,18].

However, pure copper sulfide $Cu_{2-\delta}S$ is unstable due to the evaporation of sulfur. The most resistant to uncontrolled changes in chemical composition is djurleite $Cu_{1.96}S$. It is also known that lithium doping reduces the mobility of both electronic and ionic current carriers in copper sulfide and increases the stability of the compound [8–11,19].

Over the past 12 years, copper sulfides have been intensively studied for use in thermoelectric generators [19–25]. As is known, the efficiency of a thermoelectric material is characterized by a dimensionless thermoelectric figure of merit $ZT = \sigma\alpha^2T/k$, where σ is a conductivity, α is the Seebeck coefficient, $k = k_L + k_{el}$ is a total thermal conductivity, k_L and k_{el} are a lattice and an electronic contributions correspondingly. All three kinetic coefficients, σ, α and k, depend differently on the concentration and mobility of current carriers, which makes it difficult to optimize them to achieve a high ZT semiconductor. In our opinion, for copper sulfide of stoichiometric composition at high temperatures, when the ionic component of conductivity is comparable in magnitude to the electronic component of conductivity, it is necessary to take into account the influence of ionic charge carriers on the total thermoelectric performance of the material [11]. The complex indirect effect of mixed (electron-ionic) conductivity of Cu_2S nanoclusters added to an n-type Bi_2Te_3 matrice on the thermoelectric performance was recently described by Yen et al. [26], who achieved as result of this action the recordable ZT = 1.6 at 363 K. According to Yen et al. the almost single-phase n-type crystal $Bi_2Se_{0.02}Te_3Cu_{0.03}(Cu_2S)_{0.0125}$ which they obtained with dissolved liquid-like copper chalcogenide realizes the hybridization of electronic and ionic conductivity and implements the concept of a phononic liquid electronic crystal. The presence of Cu_2S nanoclusters dynamically modulates the concentration of Cu and metallic copper ions. Cu ions play a dual role as phonon scatterers and high-mobility carriers, leading to decreased lattice thermal conductivity with increased carrier mobility. High electrical conductivity is maintained by fixing the carrier concentration at the optimal level of 10^{19} cm^{-3} with the introduction of electron donors. As we can see, the synergy of adding Cu_2S nanoclusters to bismuth telluride is great, and it seems that the development of such hybrids and nanocomposites has great prospects.

The high degree of disorder of the cationic sublattice of superionic copper sulfide, close to the "melting" state, reduces the thermal conductivity of the crystal lattice to the theoretical limit of "phonon" glass. The mobile cations in copper sulfide can be likened to a "cationic liquid" that fills the voids of the structure. The presence of a "liquid-like phase" inside a "solid" lattice interferes with the normal propagation of phonons ("phonon glass" materials) [20], therefore superionic copper chalcogenides have ultra-low lattice thermal conductivity. However, in the low-temperature non-superionic phase of copper selenide, low lattice thermal conductivity is also observed [27], which may be due to the fact that the distorted cubic lattice is retained in the low-temperature phase. Cuprous sulfide nanocrystals of 7 nm diameter synthesized with twinned structure are stable in the superionic phase well below ambient temperature [28]. Total thermal conductivity can also be reduced by a lot of methods [22–25], among it one can mark introducing impurities, micropores [29], adding a second phase [30], creation of composites and nanocomposites [23,31,32] et cetera. It may also be a productive approach to create a copper sulfide composite with a quasi-two-dimensional semiconductor with symmetry conditioning phonons with purely out-of-plane vibrational vectors to eliminate the interaction of electrons with phonons [33]. Insufficient electrical conductivity of copper sulfide can be increased by suitable doping, such as adding Al which can serve as a vacancy stabilizer as its entry into the lattice forms intensified bonds with neighboring atoms and lowers the vacancy formation energy, while reducing thermal conductivity [34].

It should be mentioned that the practical applicability of the excellent thermoelectric properties of superionic copper chalcogenides is largely a matter of discussion [35]. In 1979, research on silver-doped copper selenide was discontinued due to severe degradation of thermoelements at temperatures above 973 K as a result of rapid diffusion of copper ions [36]. However, the number of studies on the thermoelectric properties of superionic copper chalcogenides has increased many times with the advent of the age of nanotechnology. Several factors contributed to this. Firstly, the fundamental problem of increasing the thermoelectric properties of solids is interesting, and the capabilities of nanotechnology contribute to its solution. Thus, the dimensionless thermoelectric figure of merit ZT increased many times and reached, for example, an extremely high value of 2.7 for Cu_2Se nanocomposite samples [37]. New fundamental knowledge and successful methods of synthesis, heat treatment, chemistry and defect control engineering obtained with copper chalcogenides to improve thermoelectric properties can be applied to other materials, or these chalcogenides themselves can successfully work as part of composite thermoelectric materials. For example, various Cu-based superionic conductors, composited with insulating macroscale glass sheets, have been designed and fabricated, showing highly enhanced electrical stability while maintaining good thermoelectric properties [38].

Secondly, methods have been proposed to overcome or at least reduce the risk of degradation of thermoelements on base of copper chalcogenides at high temperatures. Problem of weight loss via selenium evaporation in $Cu_{1.97}Ag_{0.03}Se$ was solved via baffling of the thermoelectric leg and operation in an argon atmosphere [36]. On the basis of the analysis of copper release, a strategy for stable use was proposed by P. Qiu et al. [39]: constructing a series of electronically conducting, but ion-blocking, barriers to reset the chemical potential of such conductors to keep it below the threshold for decomposition, even if it is used with high electric currents and/or large temperature differences. For example, Schottky heterojunction between the Cu_2Se host matrix and doped BiCuSeO nanoparticles provides the accumulation of Cu^+ ions via an ionic capacitive effect at the Schottky junction under the direct current and modifies the space-charge distribution in the electric double layer, which blocks the long -range migration of Cu^+ ions and produces a drastic reduction of Cu^+ ion migration by nearly two orders of magnitude [37]. This strategy opens the possibility of using such ionic-transport-dominated materials in thermoelectric applications.

In addition, it has been shown that doping with lithium reduces the ionic conductivity of copper sulfides and selenides by several times [8,40]. An increase in the stability of the chemical composition of copper selenide at lithium doping was reported by S. D. Kang et al. [41], they achieved the high ZT = 1.4 for the $Li_{0.09}Cu_{1.9}Se$ composition at 1000 K. In addition, investigations are underway to increase the ZT of superionic thermoelectric materials in the low and medium temperature region to avoid the risks of degradation at high temperatures. This work lies in this trend of research.

It is appropriate to consider several papers devoted to the study of the thermoelectric properties of copper sulfide doped with lithium. In the work of Guan M. et al. [19], a series of $Cu_{2-x}Li_xS$ samples with various Li contents (x = 0, 0.005, 0.01, 0.05 and 0.1) were synthesized by melting-annealing. At $x < 0.05$, the $Cu_{2-x}Li_xS$ samples turned out to be stable and homogeneous at room temperature, having the same monoclinic structure as binary Cu_2S. The high zT = 0.84 at 900 K was achieved for the $Cu_{1.99}Li_{0.01}S$ composition, which is 133 % better than in pure Cu_2S. Chen E. et al. [42] studied $Cu_{4-x}Li_xS_2$ sulfides obtained by solid-state synthesis with a high lithium content (x = 1, 2, 3), which above 413 K showed isostructurality with the cubic (f.c.c.) phases Cu_2S and Li_2S. The Cu_3LiS_2 sample (or $Li_{0.25}Cu_{1.75}S$ in our terminology) showed a low thermal conductivity of 0.7 W $m^{-1}K^{-1}$ at room temperature with an increase to 0.9 W $m^{-1}K^{-1}$ at 376 K and a further sharp drop to 0.67 W $m^{-1}K^{-1}$ at 400 K, which the authors reasonably explained by disordering of copper in the lattice during the superionic transition at at 376 K.

In our earlier work [43], X-ray powder diffraction was studied on $Li_xCu_{2-x}S$ (x = 0.05; 0.10; 0.15; 0.20; 0.25) samples in the temperature range from 293 to 673 K. At room temperature, the alloys were mixtures of various modifications of copper sulfide: $Cu_{1.75}S$ orthorhombic, $Cu_{1.96}S$ tetrahedral, Cu_2S hexagonal and Cu_2S cubic systems; with increasing temperature, the number of phases decreased to one (cubic). When copper is replaced by lithium, the lattice parameter decreases almost linearly, as shown in Fig. 1a for the cubic phases of the $Li_xCu_{2-x}S$ compositions, represented from paper [43].

The ionic radius of lithium Li^+ at octahedral coordination (0.76 Å) is a little smaller than the ionic radius of copper Cu^+ (0.77 Å) [44]. A monotonic decrease in the lattice parameter with increasing lithium content (Fig. 1a) in the phase indicates the formation of a solid solution. From a fragment of the phase diagram shown in Fig. 1b for $Li_xCu_{2-x}S$ compositions with lithium content of $0.10 \leq x \leq 0.25$, it is clear that the temperature of the phase transition from the hexagonal to cubic modification is significantly reduced. Previously, we studied ionic conductivity and electron transfer in $Cu_{2-x}Li_xS$ ($x \leq 0.25$) compounds [8–10], but not measured thermal conductivity and ZT. In this work, we synthesized $Li_{0.11}Cu_{1.89}S$ composition and studied its thermoelectric and thermal properties to evaluate its potential for application in thermoelectric devices.

2. Results and discussion

Results of X-ray diffraction of the solid $Li_{0.11}Cu_{1.89}S$ sample at room temperature are shown in Table 1. X-ray phase analysis revealed the presence of three phases in the sample: monoclinic chalcocite Cu_2S, tetragonal $Cu_{1.96}S$ and monoclinic CuO. Based on the

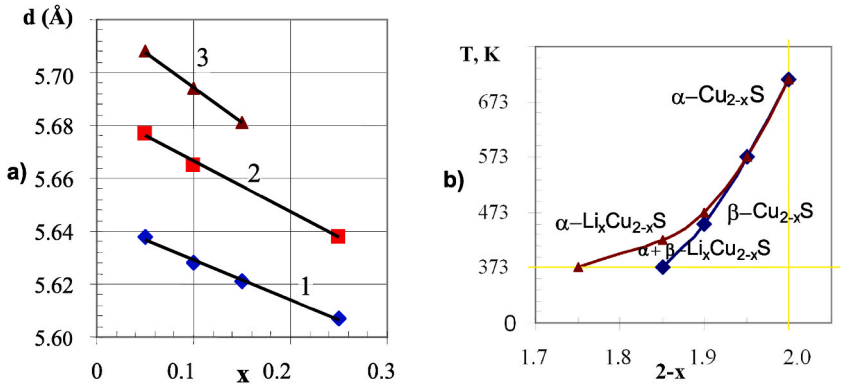

Fig. 1. Dependence of the crystal lattice parameter of the cubic phases of the $Li_xCu_{2-x}S$ compositions on the lithium content x at 473 K (1), 573 K (2), 673 K (3) temperatures (a) and a fragment of the phase diagram represented from work (b) [43]. The blue line demarcates the regions of existence of the cubic $Cu_{2-x}S$ α-phase and the hexagonal $Cu_{2-x}S$ β-phase, the red line divides the regions of the cubic phase α-$Li_xCu_{2-x}S$ and mixtures of phases (α-$Li_xCu_{2-x}S$ + β-$Li_xCu_{2-x}S$).

obtained diffraction data using the Rietveld method, the phase composition of the sample was quantitatively determined as 70.5 % of monoclinic chalcocite, 13.7 % of tetragonal $Cu_{1.96}S$ and 15.8 % of monoclinic CuO. We think that lithium is inserted into the crystal lattice without changing its structure. In Ref. [42] E. Chen et al. reported that the crystal structure of the Cu_3LiS_2 alloy at low temperatures could not be identified, but above 413 K the reflections in the powder diffraction patterns fit well with the lines of the Cu_2S cubic lattice. The proximity of the ionic radii of Li^+ (76 p.m.) and Cu^+ (77 p.m.) in a six-coordinated environment [44] should favor the solubility of lithium in the copper sulfide lattice, which is confirmed by our early works [8,43].

The lattice parameters of the monoclinic phase $Li_{0.11}Cu_{1.89}S$, as can be seen in Table 1, are a = 15.1342 Å, b = 11.7564 Å, c = 13.2617 Å; α = 90.000°, β = 116.240°, γ = 90.000°; V = 2116 Å^3. The parameters published by H. Evans [12] for low chalcocite Cu_2S are a = 15.2460 Å, b = 11.8840 Å, c = 13.4940 Å; α = 90.000°, β = 116.350°, γ = 90.000°, V = 2190 Å^3. We see a slight decrease in lattice parameters when replacing copper with lithium. Unit cell parameters of pure tetragonal Cu_2S according to A. Janosi [16]: a = 3.9960 Å, c = 11.2870 Å, V = 180.23 Å^3. According to Table 1, for the tetragonal phase $Li_{0.11}Cu_{1.89}S$ a = 3.97484 Å, c = 11.25380 Å, V = 177.80 Å^3. A slight decrease in the lattice parameters of the tetragonal phase in the sample may be due to the slightly smaller ionic radius of lithium, which replaces copper in the lattice.

Tetragonal $Cu_{2-x}S$ phase was recognized to be metastable at ambient pressure by E. H. Roseboom [14]. It is possible that the introduction of lithium makes it more stable in the case of $Li_{0.11}Cu_{1.89}S$. Potter observed the formation of a tetragonal phase of $Cu_{2-x}S$ in the electrodes of electrochemical cells at Cu:S ratio of 1.85–1.99 and between 388 and 418 K [13]. The rate of transformation to the stable phases of hexagonal chalcocite or digenite is variable and depends on composition and temperature as was found by E. H. Roseboom [14].

The third phase in the studied sample - copper oxide CuO has a monoclinic structure and, according to literature data, is stable under ambient conditions. Copper(II) oxide is a p-type semiconductor with a band gap of 1.2–2.4 eV and is promising for use in solar cells and electro-chromic devices [46,47]. CuO is believed to be intrinsically p-type with copper vacancies as acceptors being responsible for the hole conduction [48]. For CuO the lowest carrier densities are around 10^{17} cm^{-3}, which increase up to 10^{20} cm^{-3} in dependence on oxigen partial pressure. This strongly suggests that tuning the stoichiometry around the correct stoichiometric composition of the compound (oxygen poor to oxygen rich) allows the electrical conductivity and hole density to be increased, most likely due to the creation of copper vacancies [48].

In addition to X-ray diffraction analysis, DSC studies of the freshly synthesized powder were carried out in the range from 300 to 795 K in an argon atmosphere. The DSC results for the alloy are shown in Fig. 2. Two clear thermal effects were noted at 386.7 K and 737.3 K for heating. The first thermal effect begins at 378 K and ends at about 403 K, the second effect begins at about 719 K and ends at 747 K. When cooling, the peak temperatures shift to the low temperature region – to 355.8 K and to 675.2 K, as it seen on Fig. 2.

According to Kubaschewski [49], the temperatures of polymorphic transformations in copper sulfide (from the low-temperature phase to the hexagonal phase and from the hexagonal phase to the cubic phase) depend on the non-stoichiometry of the composition and correspond to temperatures of 367 and 693 K for the composition $Cu_{1.998}S$, 363 and 673 K for the composition $Cu_{1.988}S$, 365 and 589 K for $Cu_{1.9535}S$. We believe that our DSC results recorded phase transitions from the monoclinic chalcocite phase to the hexagonal phase and then from the hexagonal phase to the cubic copper sulfide phase; the presence of lithium impurities and the nanosizes of the particles may have influenced the critical temperatures of these transformations.

Fig. 3 presents images of $Li_{0.11}Cu_{1.89}S$ powder particles obtained on a scanning electron microscope. Basically, the powder contains irregularly shaped particles with seemingly melted edges. There are rods up to 15 μm long (Fig. 3c). The ends of such rods associated in

Table 1
X-ray diffraction results for the solid $Li_{0.11}Cu_{1.89}S$ sample.

2θ (deg.)	d (Å)	(hkl)	Int. (%)	FWHM (deg.)	L (Å)	Phase	Space Group	Phase concent., %	Lattice parameters	Line intensity; 2θ (on PDF card)
28.314	3.1495	−3,1,4	21,1	0.424	205	Monoclinic Cu_2S – JCPDS: 83-1462 [12]	$P2_1/c$ (14)	70.5	a = 15.1342 Å, b = 11.7564 Å, c = 13.2617 Å; α = 90.000°, β = 116.240°, γ = 90.000° V = 2116 Å^3	32.7 %; 28.23
30.303	2.9482	−5,1,2	23,3	0.273	324					35.9 %; 30.27
31.383	2.8493	−3,2,4	16,7	0.360	305					8.3 %; 31.15
32.854	2.7239	2,4,0	44,2	0.318	272					42.3 %; 32.85
35.485	2.5277	−3,4,2	31,4	0.262	341					23.5 %; 35.51
36.372	2.4684	−2, 4, 3	52,8	0.332	262					20 %; 36.36
37.456	2.3991	0,3,4	86,9	0.204	430					80 %; 37.41
38.681	2.3260	−6,2,2	24,4	0.123	729					38.3 %; 38.63
40.904	2.2052	0,5,2	19,2	0.397	226					37.5 %; 40.80
45.562	1.9893	−2,4,5	43,1	0.466	196					10.9 %; 45.49
45.999	1.9715	6,3,0	74,7	0.363	247					96 %; 45.93
48.446	1.8775	−5,3,6	100,0	0.262	347					100 %; 48.39
27.330	3.261	1,0,2	17,2	0.535	161	Tetragonal $Cu_{1.96}S$ – PDF-00-029-0578 [16]	$P4_32_12$ (96)	13.7	a = 3.97484 Å, c = 11.25380 Å, V = 177.80 Å^3	16.0 %; 27.25
31.383	2.8493	1,1,0	16,7	0.360	305					20.0 %; 31.62
39.178	2.2976	1,0,4	36,7	0.203	448					80 %; 39.10
45.562	1.9893	1,1,4	43,1	0.466	196					40.0; 45.45
35.485	2.5277	0,0,2	31,4	0.262	341	Monoclinic CuO – PDF-00-048-1548 [45]	$C2/c$ (15)	15.8	a = 4.66716 Å, b = 3.43163 Å, c = 5.12284 Å, β = 99.251°, V = 80.98 Å^3	49 %; 35.48
38.681	2.3260	1,1,1	24,4	0.123	729					96 %; 38.76

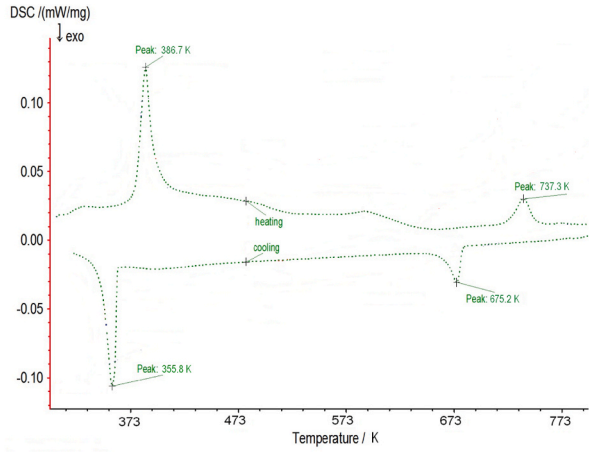

Fig. 2. Differential scanning calorimetry curves at heating and coolling of $Li_{0.11}Cu_{1.89}S$ sample in the temperature range 300–795 K.

bundles are seen on Fig. 3d. Estimated from the photo (Fig. 3a), the average particle size is 373 nm, the maximum of distribution on particle sizes corresponds to 275 nm as it seen on the diagram (Fig. 3b). The particle sizes obtained from electron microscopy are an order of magnitude higher than those estimated from X-ray diffraction. This is quite understandable, since the calculation based on the half-width of X-ray lines does not give the actual sizes of the particles, but only the sizes of the coherent scattering regions.

Fig. 4 demonstates images of the solid $Li_{0.11}Cu_{1.89}S$ surfice obtained by a scanning electron microscopy with various magnifications – ×100 (Fig. 4a), ×500 (Fig. 4b), ×5000 (Fig. 4c) and the maps of distribution of elements Cu (Fig. 4d), S (Fig. 4e), O (Fig. 4f) over the surfice area of Fig. 4b. The image Fig. 4c is a view of the part of the sample surface etched with dilute nitric acid. Blocks of about 5 μm in size and grains significantly smaller than 1 μm are visible on the surface. Also in Fig. 4c pores are noticeable. Energy dispersive X-ray

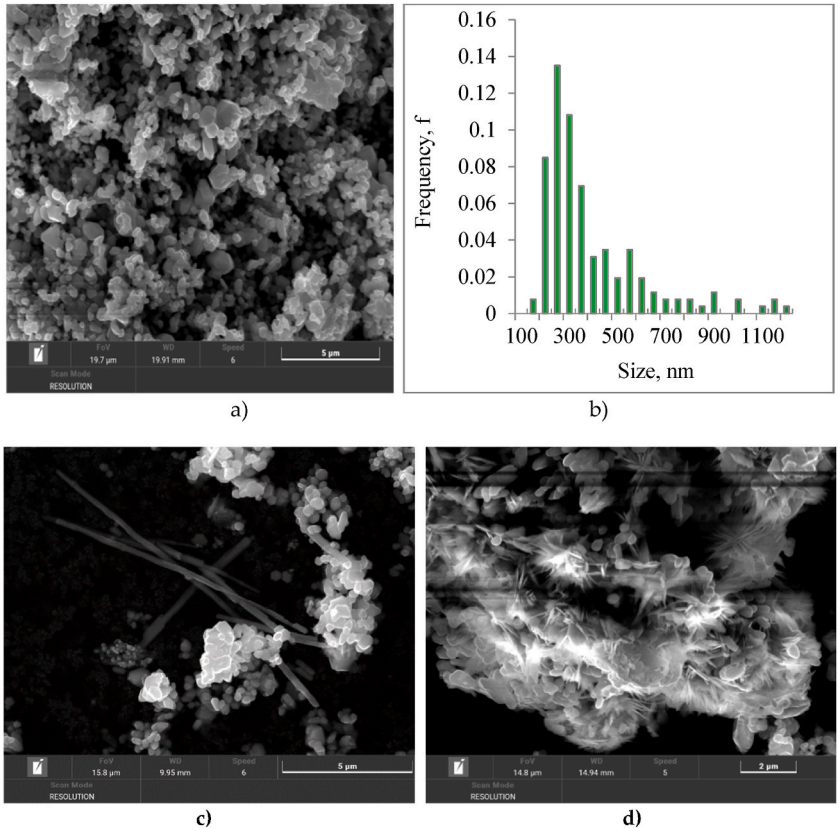

Fig. 3. Images of $Li_{0.11}Cu_{1.89}S$ powder particles obtained on a Tescan scanning electron microscope (a, c, d), the *distribution on particle sizes for* $Li_{0.11}Cu_{1.89}S$ *powder (b).*

analysis showed the presence of three elements in the $Li_{0.11}Cu_{1.89}S$ solid sample - copper, sulfur and oxygen. Lithium is not detected by energy dispersive X-ray analysis due to its low atomic number. The content of elements in atomic percent is given in Table 2.

Simplistically assuming that copper is distributed over the $Cu_{1.89}S$ and Cu_xO phases, we obtain from the analysis of the data presented in Tables 2 and $x \approx 1$ with an error of up to 5 %. Taking into account our simplification and the fact that EDS was carried out locally and not over the entire surface of the sample, we can assume that EDS confirms the results of X-ray phase analysis.

Fig. 5 presents the temperature dependences of the electronic conductivity (a) and electronic Seebeck coefficient (b) of the $Li_{0.11}Cu_{1.89}S$ alloy.

The electronic conductivity of the $Li_{0.11}Cu_{1.89}S$ alloy at room temperature is 46 S/cm, which is much higher than the value of 11 $S{\bullet}cm^{-1}$ for stoichiometric Cu_2S [19], and it gradually increases to a maximum of 182 $S{\bullet}cm^{-1}$ at 563 K, exhibiting semiconductor properties. The electronic conductivity of the $Li_{0.05}Cu_{1.95}S$ composition at room temperature, measured in Ref. [19], has a value of 87 $S{\bullet}cm^{-1}$, increasing to approximately 125 $S{\bullet}cm^{-1}$ near 375 K. The content of copper oxide in our sample is small (15.8 wt%, as seen in Table 1), so we believe that the conductivity of the $Li_{0.11}Cu_{1.89}S$ alloy is determined by the lithium-doped copper sulfide phase, especially since the conductivity of copper oxide is much lower than that of the sulfide ($\sim 1{,}4 \times 10^{-5}$ $S{\bullet}cm^{-1}$ at 300 K [50]).

Thus, the lithium insertion into the lattice of Cu_2S greatly increases the conductivity of the semiconductor. It is reasonable to believe that lithium plays the role of a donor impurity, creating impurity levels in the band gap of the semiconductor. However, the conduction electrons generated during the ionization of lithium impurity atoms are compensated by electron holes caused by the ionization of copper vacancies in the cation sublattice. If the concentration of lithium atoms in the sites of the cationic sublattice coincides with the concentration of vacant copper positions in the $Cu_{2-x}S$ lattice, the $Li_xCu_{2-x}S$ semiconductor can be considered as a fully compensated semiconductor with acceptor (copper vacancies) and donor (lithium atoms) impurities. Since in this case the semiconductor remains hole-conducting, but the conductivity increases, it can be assumed that the compensation is partial, and the concentration of holes significantly exceeds the concentration of electrons in the conduction band. Possible scenarios for defect formation in $Li_xCu_{2-x}S$ ternary alloys require special investigation.

The temperature dependences of the conductivity of $Li_xCu_{2-x}S$ samples ($x = 0.005, 0.010, 0.050$) in the work of M. Guan et al. [19] display a second, local maximum, which position is shifted towards lower temperatures with increasing lithium content. The maximum for the $Li_{0.05}Cu_{1.95}S$ composition is observed near 620 K (Fig. 5a). For our $Li_{0.11}Cu_{1.89}S$ sample, a similar conductivity maximum is shifted to 570 K, which follows to the general trend of lithium doping in copper sulfide. We consider that the beginning of a decline in conductivity at 570 K is caused by a gradual change in the structure leading to the transition to the cubic phase of copper sulfide at 670

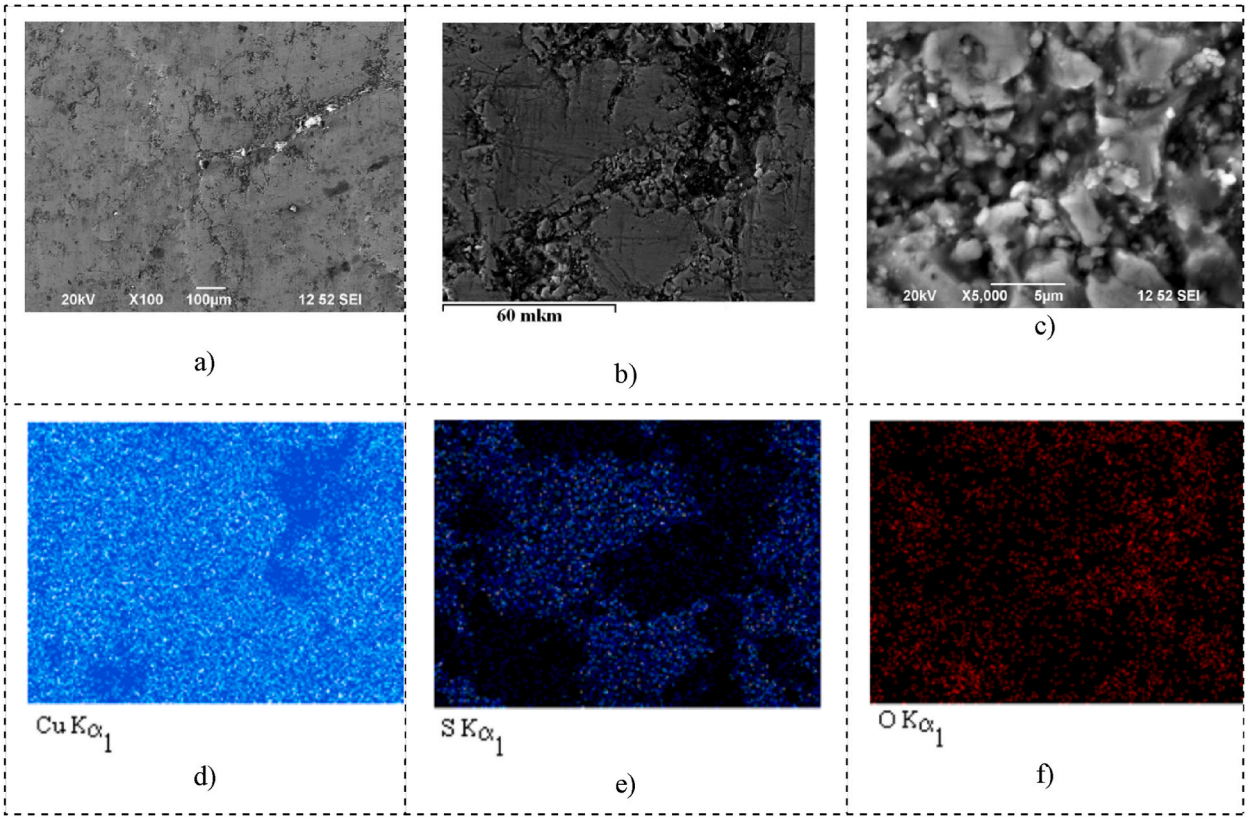

Fig. 4. Images of the solid $Li_{0.11}Cu_{1.89}S$ surfice obtained by a scanning electron microscopy (a, b, c) with various magnifications. The maps of distribution of elements Cu (d), S (e), O(f) were taken over the surfice area of Fig. 4b.

Table 2
Spectral analysis results for $Li_{0.11}Cu_{1.89}S$ sample.

Element	Cu	S	O
Content, at. %	62.78	23.87	13.35

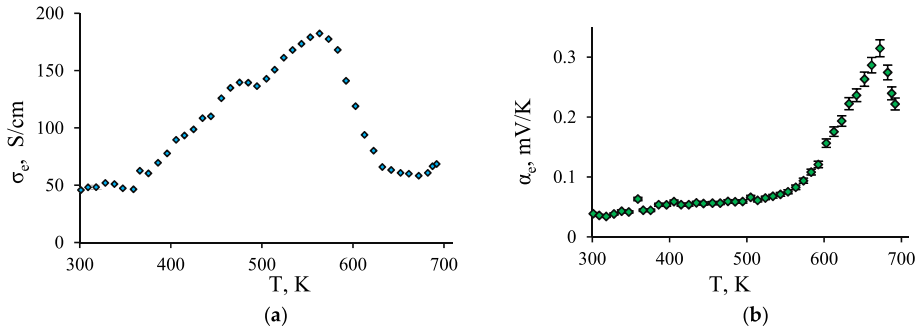

Fig. 5. The results of electronic transport studies in the $Li_{0.11}Cu_{1.89}S$ alloy: (**a**) The temperature dependence of the electronic conductivity; (**b**) The temperature dependence of the electronic Seebeck coefficient.

K, which is characterized by low conductivity less than 1 S•cm^{-1} [2,4]. Copper sulfide and selenide are characterized by a constant redistribution of cations over the tetrahedral, octahedral and trigonal voids of the rigid anion lattice framework with increasing temperature [51,52], which can also affect the conditions of electron transfer, in particular, the mobility and effective mass of carriers.

The small jump in the conductivity of $Li_{0.11}Cu_{1.89}S$ at 366 K in Fig. 5a most likely is caused by the phase transition from monoclinic chalcocite Cu_2S to hexagonal chalcocite. The calculated value of the activation energy is 0.14 ± 0.01 eV in the range 405–563 K. This value is slightly higher than in binary copper sulfide - for the low-temperature phase of copper sulfide in the work of Sorokin et al. [2] an activation energy of 0.09 eV was obtained in the temperature range from 250 up to 673 K.

Around 570 K, the maximum conductivity in Fig. 5a corresponds to the almost minimum Seebeck coefficient. Near the point 570 K, a strong decrease in conductivity begins, accompanied by a strong increase in the Seebeck coefficient, as seen in Fig. 5b. Conductivity and Seebeck coefficient are coupled through the Fermi level and behave as usual in semiconductors. A clearly expressed minimum of the Seebeck coefficient at 570 K may be absent due to the influence of the second phase of the compound.

The maximum Seebeck coefficient is obviously achieved when the predominant type of conductivity changes: the impurity conductivity caused by the ionization of cation vacancies and lithium impurities reaches saturation, and the generation of electron-hole pairs begins due to the transfer of electrons through the energy gap (intrinsic conductivity develops). The increase in the Seebeck coefficient with heating, inherent in a degenerate semiconductor, is replaced by a decrease due to compensation of the hole contribution to Seebeck coefficient due to (bipolar) intrinsic conductivity.

In work [14], a decrease in the Seebeck coefficient of $Li_xCu_{2-x}S$ samples was noted with increasing lithium content x. For Cu_2S, Guan et al. [14] obtained $\alpha \approx 0.3$ mV/K, and for $Li_{0.05}Cu_{1.95}S$ sample the Seebeck coefficient is 0.08 mV/K. The electronic Seebeck coefficient of our sample is about 0.04 mV/K at room temperature, what is a reasonable result in light of previous sentence. It increases slightly with temperature which is typical for a degenerate semiconductor, up to approximately 570 K. The sign of the coefficient is positive for the sample, indicating the hole type of conductivity. Above 570 K, the Seebeck coefficient begins to increase strongly, achieving a maximum of 0.31 mV/K at 672 K.

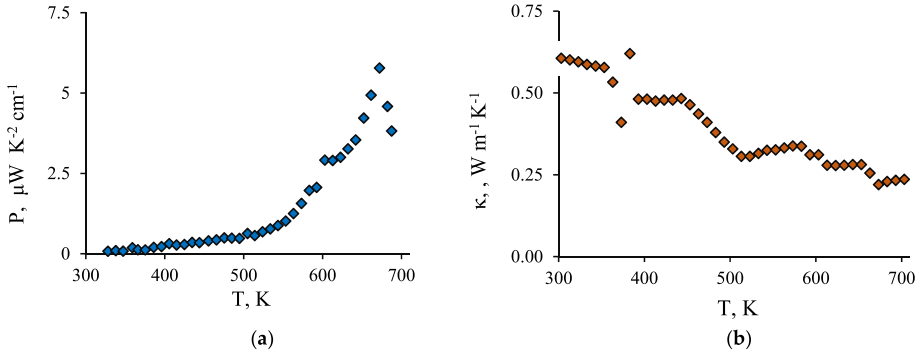

Fig. 6. The temperature dependence of the power factor $P = \sigma_e\alpha_e^2$ for the $Li_{0.11}Cu_{1.89}S$ alloy (**a**); The temperature dependence of the total thermal conductivity of the $Li_{0.11}Cu_{1.8\ 9}S$ alloy (**b**).

The position of the maximum of the Seebeck coefficient corresponds to the position of the Fermi level of electrons at the band edge [53]. A state of intrinsic conductivity, in which the Fermi level is located in the middle of the energy gap, for copper sulfide is attained in the cubic phase [4,6]. Thus, the Fermi level at 672 K is in a state of movement upward towards the middle of the gap. We believe that the Fermi level, with increasing temperature, crosses a narrow Li impurity band located inside the energy gap of the semiconductor; this explains the observed extremes of electronic conductivity and the Seebeck coefficient.

The temperature dependence of a power factor $P = \sigma_e\alpha_e^2$ of the $Li_{0.11}Cu_{1.89}S$ alloy is shown in Fig. 6 (a). It has a sharp maximum of 5.8 μW $K^{-2}cm^{-1}$ at 672 K, coinciding in position with the maximum of the Seebeck coefficient. For comparison, in the work of M. Guan et al. [14], for the $Li_{0.05}Cu_{1.95}S$ composition, a maximum value of the power factor of 6.4 μW $K^{-2}cm^{-1}$ at 800 K was obtained.

The temperature dependence of the thermal conductivity of $Li_{0.11}Cu_{1.89}S$ was measured in the range from room temperature to 700 K. It is shown in Fig. 6 (b). Thermal conductivity has a maximum value of 0.61 W $m^{-1}K^{-1}$ at room temperature and decreases to 0.22 W•$m^{-1}K^{-}$at 673 K. Sharp peak is observed at 378 K vicinity, caused by phase transition from monoclinic chalcocite Cu_2S to hexagonal chalcocite.

From the total thermal conductivity, by subtracting the electronic component of thermal conductivity $k_{el.}$, calculated according to the Wiedemann - Franz law, the lattice thermal conductivity k_L of the alloy was determined, shown in Fig. 7a. To determine $k_{el.}$ values the temperature dependence of Lorenz number was used, which was calculated for $Li_{0.05}Cu_{1.95}S$ sample by Guan et al. [19]. It can be seen that the lattice thermal conductivity experiences a small jump-like drop around 370 K, which corresponds to a phase transition to the superionic hexagonal phase of copper sulfide (this jump is also visible in Fig. 6b for the total thermal conductivity). Further, the lattice thermal conductivity decreases quite quickly with increasing temperature to approximately 524 K achieving 0.14 W•$m^{-1}K^{-1}$, then experiences weak changes between 0.15 and 0.21 W•$m^{-1}K^{-1}$.

Extremely low thermal conductivity was previously observed in a number of studies for pure copper sulfide. According to the work of Y. He et al. [54], the reason for the low lattice thermal conductivity of copper sulfide is the switching off of transverse modes, which leads to a decrease in κ_L compared to conventional amorphous solids.

The advantages of liquid-like copper ions for high thermoelectric performance include very strong phonon scattering as well as the additional reduction of specific heat due to the suppression of transverse phonon modes [54]. The minimum thermal conductivity κ_{min} calculated from the high temperature limit of Cahill's formula [55].

$$k_{min} = \frac{1}{2}\left(\frac{\pi}{6}\right)^{1/3} kV^{-2/3}\left(2v_{tr.} + v_{long.}\right), \quad (1)$$

where $\upsilon_{tr.}$ and υ_{long} are average transverse and longitudinal speeds of sound, gives a good estimate for the lattice thermal conductivity when all phonons (transverse and longitudinal) completely scattered. If some shear modes (approximately half) are removed from the Cahill's formula (1), we have values usual for superionic liquid-like lattice of copper sulfide, below that of glasses or other normal amorphous solids [54].

Factors that reduce thermal conductivity in our case are also the heterophase nature of the alloy, the presence of a high impurity concentration (Li, O) and a large scatter in the sizes of particles of the main phase and inclusions of impurity phases, which further reduces the overall lattice thermal conductivity lower than the already low intragranular thermal conductivity of the superionic copper sulfide. In the recent works of Bulat et al. [56,57], it was found that the experimental values of thermal conductivity (0.2 W•$m^{-1}K^{-1}$) in nanostructured samples of copper selenide are significantly lower than those given by theoretical calculations. Extremely low lattice thermal conductivity is due to phonon scattering at intergrain nanoboundaries and nanodefects. For example, S. Singh et al. [58] achieved a drastic reduction in the values of k from ~0.88 W/mK to ~0.23 W/mK as crystallite size is reduced from 49 nm to 20 nm at ~600 K. Extremely low thermal conductivities 0.1 ÷ 0.3 W•$m^{-1}K^{-1}$ were obtained also by Balapanov et al. [59] for nanocrystalline $Na_{0.15}Cu_{1.85}S$.

It is known that in the micro- and nanoscale regime the thermal conductivity is lower than that of the bulk materials. For example, it was found, through solving the Boltzmann transport equation of heat carrier in the host medium, that heat transfer surrounding a nanometer-size particle whose mean free path is on the order of its physical dimension is reduced and localized heating occurs [60].

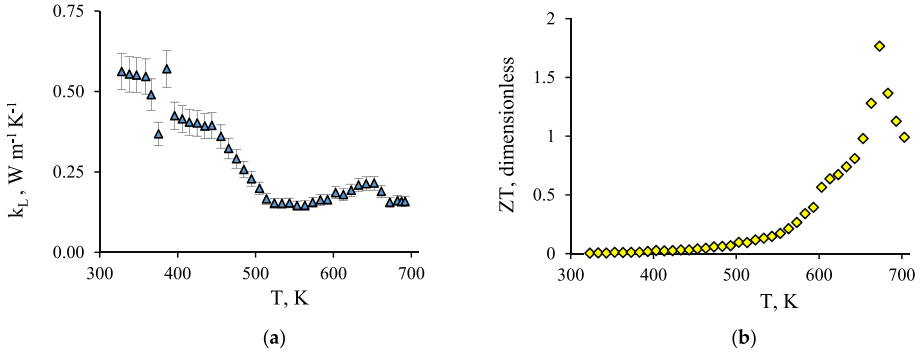

Fig. 7. The temperature dependences of the lattice thermal conductivity (**a**) and dimensionless thermoelectric figure of merit $ZT = \sigma_e\alpha_e^2T/k$ for the $Li_{0.11}Cu_{1.89}S$ alloy.

Based on the results of measurements of transfer coefficients, the dimensionless thermoelectric figure of merit $ZT = \sigma_e\alpha_e^2T/k$ were calculated, shown in Fig. 7 b. It can be seen that at 672 K the ZT value reaches 1.76, which is a significant achievement for this temperature. This highest result is achieved at the phase transition point in copper sulfide. Considering that at this moment one part of the sample is in the hexagonal phase, and the other is in the cubic phase (the temperature difference between the measuring probes is about 10°), we find an analogy with earlier works [17,18] those studied the colossal Seebeck effect during the phase transition from non-superionic to superionic modification of copper selenide and copper sulfide. We believe that dynamical variation of carrier concentration leading to the large Seebeck coefficient [18] is a possible reason for the high thermoelectric performance.

The achieved high ZT value for $Li_{0.11}Cu_{1.89}S$ allows to propose its use as a p-leg in monolithic thermoelectric generators similar to described ones in papers [61,62] in pair with ductile n-type $Ag_2S_{0.55}Se_{0.45}$ compound, for example. Commercially available thermoelectric generators (TEGs) usually consist of expensive and toxic Bi_2Te_3-based thermoelectric materials and are difficult to fabricate. As an alternative proposal, the authors of [62] developed a monolithic TEG based on Ag and Cu chalcogenides using a facile device fabrication process for low-grade waste heat recovery. They used ductile $Ag_2S_{0.55}Se_{0.45}$ and superstoichiometric $Cu_{2.075}Se$ with a zT value of ~0.5 at 300 K. By optimizing the device fabrication process, they were able to assemble monolithic TEGs without the significant effect of Ag or Cu ion migration. In Ref. [62], the maximum power density of 0.68 mW/cm^2 at $\Delta T = 30$ K was obtained, which is comparable to a similar monolithic TEG based on Bi_2Te_3. These results indicate that monolithic TEGs based on copper and silver chalcogenides can be a simple and low-cost alternative to Bi_2Te_3-based TEGs for energy harvesting applications.

To optimize the lithium and copper content in $Li_xCu_{2-\delta}S$ composition in order to increase ZT, one can further take advantage of the controlled electrochemical insertion of lithium and copper ions into the sample, using ion filters or immersing the sample in an electrolyte for a certain time [63].

The presence of copper oxide in the composite was not initially planned. Since significant copper oxide formation occurred during the synthesis and sample preparation process, we must also discuss its possible impact on the obtained ZT value. High-purity CuO possesses a beautiful Seebeck coefficient α (~0.6 mV/K at 300 K), but exhibits both too poor electrical conductivity (~1.4×10^{-5} S•cm^{-1} at 300 K) and a too high thermal conductivity (~40 W•$m^{-1}K^{-1}$ at 300 K) [50] to be suitable for thermoelectric applications. However, composites with a small amount of Cu_2S in bulk CuO exhibits significantly better electrical conductivity (~10^1 S•cm^{-1} at 300 K) and lower thermal conductivity (~35 $Wm^{-1}K^{-1}$ at 300 K), resulting in power factor increasing from 10^{-10} W•$m^{-1}K^{-2}$ for pure CuO to 10^{-5} W•$m^{-1}K^{-2}$ for the CuO/Cu_xS composite [64].

It is clear that the presence of poor conductive copper oxide in our alloy cannot improve the electrical conductivity of the material. However, the total Seebeck coefficient of the composite can be increased by the presence of the CuO impurity phase with a high α~0.6 mV/K, including due to the effect of energy filt ration of carriers at phase boundaries. It is more difficult to explain why the overall thermal conductivity of the composite turned out to be so low, despite the presence of a noticeable concentration (15.6 %) of a phase with a very high thermal conductivity of ~40 W•$m^{-1}K^{-1}$. It is possible that the concentration of copper oxide impurity in the sample under study still does not reach the critical threshold at which the total thermal conductivity of the alloy would become as high as in CuO. We believe that CuO particles are mainly surrounded by copper sulfide particles with low thermal conductivity and do not form continuous chains, as a result of which they cannot have a significant effect on the total heat transfer in the sample. At the same time, the presence of a second phase in the sample always reduces a total thermal conductivity due to the appearance of additional interphase boundaries at which phonon scattering occurs.

Also it is must be noticed that Li^+ have a comparable size to Cu^{2+}(0.73 Å) and may be preferable for occupying the vacancy site of Cu in CuO lattice or to replace the Cu^{2+} site in CuO. Yoshida et al. [50] reported that for Li-doped copper oxide ($Cu_{1-x}Li_x$)O, the electrical conductivity increased and Seebeck coefficient α decreased with increasing Li-content up to x = 0.03. Seebeck coefficient showed excellent values 0.3–0.4 mV/K at temperature range 270–700 K) [50]. The electrical conductivity of $Li_{0.03}Cu_{0.97}O$ is about 2.6 S/cm at 340 K and 12.8 S/cm at 700 K. Power factor achieves a high value of 10^{-4} W•$m^{-1}K^{-2}$ for $Li_{0.03}Cu_{0.97}O$ at 700 K. Thus, the fact of such a successful accidental doping of copper oxide with lithium, the presence of which in this composition with low thermal conductivity was also not initially expected, could improve the thermoelectric performance of the material under study. It is unlikely that this took place in our case, but, probably, a special study of the properties of such a $Li_xCu_{2-x}S$ - ($Cu_{1-x}Li_x$)O composite would make sense.

3. Materials and methods

A sample of the chemical composition $Li_{0.11}Cu_{1.89}S$ was synthesized in a melt of a mixture of NaOH and KOH hydroxides at about 438 K using LiCl, CuCl, and Na_2S*9H_2O as reagents. A mixture of hydroxides NaOH and KOH is used as ion-transporting, non-consumable medium for the reaction. The annealing time was 12 h. The product obtained in the form of a clot was washed three times with distilled water, then with pure ethanol, and then dried at room temperature.

X-ray diffraction phase analysis was carried out using the Bruker D8 ADVANCE ECO diffractometer with a Cu-K_α radiation and a graphite filter. Diffraction patterns were recorded with step 0.03° (2θ). To identify the phases the BrukerAXSDIFFRAC.EVAv.4.2 software and the international ICDD PDF-2 and COD databases were used.

The Scherrer equation was used to determine the mean size of coherently scattering domains (CSD).

Based on the obtained diffraction patterns using the Rietveld method, the phase composition of the synthesized samples was quantitatively determined.

Differential scanning calorimetry (DSC) was carried out on a DSC 404 F1 Pegasus device from NETZSCH in an argon atmosphere. The particle sizes of the synthesized powder were assessed using a Tescan scanning electron microscope.

Rectangular tablets 3 × 3 × 20 (mm) for kinetic measurements were pressed from the $Li_{0.11}Cu_{1.89}S$ powder under a pressure of 3

ton/cm^2. Temperature dependences of the electronic conductivity and electronic Seebeck coefficient were measured simultaneously in argon atmosphere. For measurements of electronic conductivity, a four-probe method using direct current was used (see Fig. 8a).

The technique for measurements of partial electronic conductivity in a mixed electron-ion conductor is described in the works of M. Hebb [65] and I. Iokota [5,66]. When a direct current is passed through contacts 1–2 (Fig. 8a), the ion current is blocked at the sample boundaries by inert graphite electrodes, which leads to the concentration polarization. At the moment the current is turned on, all charge carriers (holes and Cu^+ ions) participate in conductivity, at this moment the conductivity is the sum of the ionic and electronic conductivities $\sigma_0 = \sigma_i + \sigma_e$, but over time the flow of cations to the cathode under the action of the applied electric field is balanced by the reverse diffusion flow of Cu^+ cations caused by the resulting cation concentration gradient. Thus, in a steady state, the current in the sample is carried only by electronic holes. When turning DC current on and off through contacts 1–2 of Fig. 8a, the concentration polarization in the sample establishes and decreases (see Fig. 8b). At the moment the current is turned on the potential difference between probes 3–4 is described by the formula

$$U_0 = \frac{IL}{S(\sigma_i + \sigma_e)} \ . \tag{2}$$

equation (2) shows that initially the potential difference between 3 and 4 electronic probes is caused by both electronic and ionic conductivities. In a steady state, the potential difference U_∞ between electronic probes 3–4 is described by the expression:

$$U_\infty = \frac{k_B T}{e} \ln \frac{1+a}{1-a}, \tag{3}$$

in which the symbol a denotes

$$a = \frac{eIL}{2Sk_B T\sigma_e} \ . \tag{4}$$

In equation (4) symbols e, I, L, S, k_B, T, σ_e are the charge of the electron, the current, the length of the sample, the cross section of the sample, Boltzmann's constant, the temperature and the electronic conductivity correspondingly.

For $a \ll 1$, we have from equation (3) taking into account equation (4) the usual formula expressing Ohm's law:

$$U_\infty = \frac{IL}{\sigma_e S} \ . \tag{5}$$

Thus, to correctly determine conductivity using equation (5), the condition of small current $a \ll 1$ and the condition of achieving an equilibrium state must be met. The polarization phenomenon can be neglected if $\sigma_e \gg \sigma_e$.

The electronic Seebeck coefficient was measured by C. Wagner's method [67] in the same measuring cell (Fig. 8a) in the absence of current. The temperature gradient was about 8 K/cm. To eliminate the influence of thermoelectric force ($U_{therm.}$) on the result of conductivity measurements, two measurements (U^+ and U^-) were carried out in opposite directions of current, and then Ohm's voltage was calculated as $U = [(U^+ + U_{therm.}) - (U^- - U_{therm.})]/2 = (U^+ - U^-)/2$. The chromel branches of the chromel - alumel thermocouples were used as inert electronic potential probes 3–4 (Fig. 8a) for measuring of ohmic potential difference and thermo-electric force. The error in conductivity measurements was 3–4%, one in the Seebeck coefficient measurements was 4–5%.

If a temperature gradient is applied to a semiconductor in an open circuit (Fig. 8a), a potential difference arises along its length due to the diffusion of current carriers from the heated end to the cold (Seebeck effect). After establishing a state of thermodynamic equilibrium in the sample the potential difference between contacts 3–4 contains, in addition to the Seebeck e.m.f. in the sample under study, the contribution of the Seebeck effect in metal wires $U_{metal.}$ and the contribution $U_{cont.}$, caused by dependence of the contact potential difference on temperature:

$$U = U_{Seebeck} + U_{metal.} + U_{cont.} \tag{6}$$

The contact component in equation (6) can be reduced to almost zero by choosing the same wire material. The Seebeck effect $U_{metal.}$

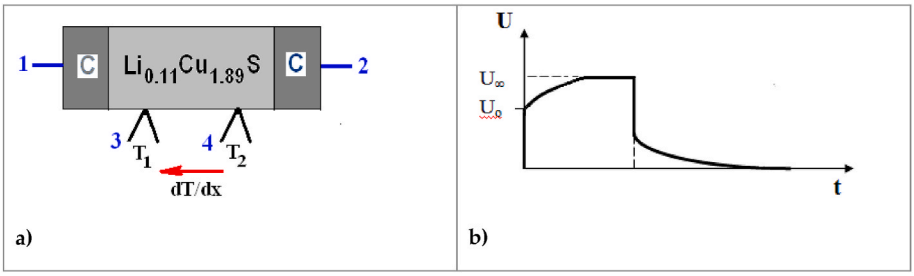

Fig. 8. Scheme of the electrochemical cell for measurements of the electronic conductivity and electronic Seebeck coefficient (a) and time dependence of potential difference between 3 and 4 electronic probes (b) when direct current impulse pass through the C/$Li_{0.11}Cu_{1.89}$S/C cell shown on left figure.

in the measuring wires can usually be neglected compared to the Seebeck effect in the volume of the sample, but it can be easily calculated and subtracted from the total thermo-e.m.f. U when this contribution is significant. The Seebeck coefficient of a sample is determined as

$$\alpha_e = \lim_{\Delta T \to 0} \frac{U(T, T+\Delta T)}{\Delta T} = \frac{dU}{dT} \tag{7}$$

The studied potential difference U_e measured between the electron probes (contacts 3, 4 in Fig. 8a) can be written in the form

$$\Delta U_e = j^3 - j^4 = -\frac{1}{e}\left(\eta_e^4 - \eta_e^3\right), \tag{8}$$

if we neglect the temperature dependence of the electron chemical potential. Under conditions of local thermodynamic equilibrium, the following expressions are valid for the chemical potentials of electrons in the sample at temperatures T_1 and T_2:

$$\eta_e^3 = \eta_e^{Li_{0.11}Cu_{1.89}S}(T_1), \tag{9}$$

$$\eta_e^4 = \eta_e^{Li_{0.11}Cu_{1.89}S}(T_2), \tag{10}$$

After substituting equations (9) and (10) into equation (8), latter takes the form

$$\Delta U_e = -\frac{1}{e}\left(\eta_e^{Li_{0.11}Cu_{1.89}S}(T_2) - \eta_e^{Li_{0.11}Cu_{1.89}S}(T_1)\right), \tag{11}$$

and accordingly to equation (7), taking into account equation (11) the electron Seebeck coefficient can be expressed as

$$\alpha_e = \lim_{\Delta T \to 0} \frac{\Delta U_e}{\Delta T} = \frac{d\eta_e^{Li_{0.11}Cu_{1.89}S}}{dT}\ . \tag{12}$$

From equation (12) it is clear that the coefficient is determined only by the gradient of the chemical potential of the electrons in the sample. Thus, using unipolar electronic inert probes for measurements, it is possible to measure the electronic Seebeck coefficient in a mixed electron-ionic conductor.

Thermal conductivity measurements were performed using the flash method on an LFA 467 HT HyperFlash device (NETZSCH, Germany). Thermal conductivity was found from three measurements:

$k(T) = D(T) \bullet \rho(T) \bullet c_p(T)$,

where T is the temperature, k is the thermal conductivity, D is the thermal diffusivity, ρ is the bulk density, c_p is the specific heat capacity.

Thermal diffusivity was measured on LFA 467 HT device using the Parker formula from an analysis of the time dependence of the temperature of the opposite side of the sample after short-term heating of one side of the sample with a powerful light pulse. The heat capacity values c_p were determined on a DSC calorimeter DSC 404 F1 Pegasus (NETZSCH, Germany) in an argon atmosphere. The density of the sample ρ was found from measurements of the weight and sample volume. The measurements were performed in an argon atmosphere.

The error in thermal conductivity measurements was 10–12 %.

4. Conclusions

The thermoelectric material is a mixture of monoclinic Cu_2S and tetragonal $Cu_{1.96}S$ phases at room temperature. The average particle size of the synthesized powder is about 373 nm. Differential scanning calorimetry revealed thermal effects around 386 K and 737 K at heating (356 K and 675 K at cooling), roughly corresponding to phase transitions from the monoclinic chalcocite phase to hexagonal one and then to cubic phase of copper sulfide; the presence of lithium impurity and the nanosize of the particles somewhat changed the critical temperatures of these transformations. X-ray analysis revealed the presence of CuO impurity phase in solid sample at room temperature.

The electronic conductivity of the alloy has a semiconductor character from room temperature to 563 K with an activation energy of 0.14 ± 0.01 eV. According to the sign of the Seebeck coefficient, electronic conduction is carried out by holes. The electronic Seebeck coefficient at room temperature is 0.04 mV/K and increases with temperature, which is typical for a degenerate semiconductor. However, above 570 K, a strong increase in the Seebeck coefficient begins, which we associate with the beginning of structural transformations into the cubic phase of copper sulfide. The maximum Seebeck coefficient 0.31 mV/K provides a high power factor of 5.8 $\mu W \bullet K^{-2}\, cm^{-1}$ at 672 K. Maximal power factor is achieved at the phase transition point in copper sulfide. Considering that at this moment one part of the sample is in the hexagonal phase, and the other is in the cubic phase, we find an analogy with earlier work that studied the colossal Seebeck effect during the phase transition from non-superionic to superionic modification of copper selenide. We believe that dynamical variation of carrier concentration leading to the large Seebeck coefficient [18] is a possible reason for the high thermoelectric performance. Analysis of the possibility of influence of CuO impurity on the thermoelectric performance of the alloy under study shows that the probability of the significant influence can be considered negligible.

The total thermal conductivity has very low values, typical for materials such as "phonon glasses". It gradually decreases from 0.61 $W \bullet m^{-1}K^{-1}$ at room temperature to 0.22 $W \bullet m^{-1}K^{-1}$ at 673 K. The lattice thermal conductivity shows a abrupt peak at 378 K vicinity, which corresponds to the phase transition from the monoclinic structure to the superionic hexagonal structure of copper sulfide. Such the low thermal conductivity and high Seebeck coefficient provide high ZT = 1.76 at 672 K, which is a considerable achievement for this temperature, and allows us to classify the $Li_{0.11}Cu_{1.89}S$ alloy as a promising thermoelectric material.

CRediT authorship contribution statement

Marzhan Kubenova: Writing – original draft, Project administration, Methodology, Investigation. **Malik Balapanov:** Validation, Supervision, Resources, Methodology, Investigation, Formal analysis, Conceptualization. **Kairat Kuterbekov:** Software, Resources, Project administration, Data curation. **Rais Ishembetov:** Software, Investigation, Conceptualization. **Rafail Almukhametov:** Visualization, Validation. **Kenzhebatyr Bekmyrza:** Visualization, Conceptualization. **Bulat Akhmetgaliev:** Investigation. **Talgat Sharipov:** Formal analysis. **Marat Zeleev:** Software, Investigation. **Asset Kabyshev:** Validation. **Zhamal Mukhanova:** Investigation. **Bakhytkul Baikhozhaeva:** Formal analysis. **Robert Yakshibaev:** Methodology.

Informed consent statement

Not applicable.

Institutional review board statement

Not applicable.

Data availability statement

Not applicable.

Funding

This research was funded by Science Committee of the Republic of Kazakhstan, which is part of the Ministry of Science and Higher Education, grant number "AP14871197".

Declaration of competing interest

The authors declare the following financial interests/personal relationships which may be considered as potential competing interests:

Kubenova Marzhan reports financial support was provided by L N Gumilyov Eurasian National University. Kubenova Marzhan reports a relationship with L N Gumilyov Eurasian National University that includes: employment and funding grants. Kubenova Marzhan has patent No pending to No. The authors declare that there are no competing interests or financial conflicts related to this research. All funding sources have been acknowledged in the manuscript.

The authors declare that they have no known competing financial interests or personal relationships that could have appeared to influence the work reported in this paper.

If there are other authors, they declare that they have no known competing financial interests or personal relationships that could have appeared to influence the work reported in this paper.

References

[1] E. Hirahara, The physical properties of cuprous sulfides – semiconductors, J. Phys. Soc. Jpn. 6 (1951) 422–427, https://doi.org/10.1143/jpsj.6.422.
[2] G.P. Sorokin, A.P. Paradenko, Electrical properties of Cu_2S, Soviet phys. J. Izv. Vuzov. Fizika (USSR) 9 (1966) 59–61, https://doi.org/10.1007/BF00818183.
[3] O.P. Astakhov, V.V. Lobankov, Seebeck coefficient and electrical conductivity of copper chalcogenides, Teplofizika vysokikh temperatyr (USSR). 10 (4) (1972) 905–906. https://www.mathnet.ru/php/getFT.phtml?jrnid=tvt&paperid=9754&what=fullt&option_lang=rus.
[4] K. Okamoto, Sh Kawai, Electrical conduction and phase transition of copper sulfides, Jap. J. Appl. Phys. 12 (1973) 1130–1138, https://doi.org/10.1143/jjap.12.1130.
[5] I. Iokota, On the theory of mixed conduction with special reference to conduction in silver sulfide group semiconductors, J. Phys. Soc. Jpn. 16 (1961) 2213–2223, https://doi.org/10.1143/jpsj.16.2213.
[6] R. Marshall, S.S. Mitra, Optical properties of cuprous sulfide, J. Appl. Phys. 36 (1965) 3882–3883, https://doi.org/10.1063/1.1713966.
[7] R.A. Yakshibaev, M.K. Balapanov, V.N. Konev, Ionic conductivity and diffusion in superionic conductor Cu_2S, Fizika Tverdogo Tela (USSR) 28 (1986) 1566–1568.
[8] M.Kh Balapanov, I.G. Gafurov, U.Kh Mukhamed'yanov, R.A. Yakshibaev, R.Kh Ishembetov, Ionic conductivity and chemical diffusion in superionic $Li_xCu_{2-x}S$ ($0 \leq x \leq 0.25$), phys. stat. sol. (b). 241 (2004) 114–119, https://doi.org/10.1002/pssb.200301911.
[9] R.Kh Ishembetov, M.Kh Balapanov, Y.Kh Yulaeva, Electronic peltier effect in $Li_xCu_{(2-x)-\delta}S$, Rus. J. Electrochem. 47 (2011) 416–419, https://doi.org/10.1134/S1023193511040070.
[10] M.Kh Balapanov, R.Kh Ishembetov, E.K. Urazaeva, R.A. Yakshibaev, K.A. Kuterbekov, T.N. Nurakhmetov, Influence of the cation sublattice defectness on the electronic thermoelectric power of $Li_xCu_{(2-x)-\delta}S$ ($0 \leq x \leq 0.25$), Inorg. Mater. 50 (2014) 930–933, https://doi.org/10.1134/S1023193511040070.

[11] M.M. Kubenova, K.A. Kuterbekov, M.Kh Balapanov, R.Kh Ishembetov, A.M. Kabyshev, K.Z. Bekmyrza, Some thermoelectric phenomena in copper chalcogenides replaced by lithium and sodium alkaline metals, Nanomaterials 11 (2021) 2238–2286, https://doi.org/10.3390/nano11092238.
[12] H.T. Evans jr., The crystal structures of low chalcocite and djurleite, Z. Kristallogr. 150 (1979) 299–320, https://doi.org/10.1524/zkri.1979.150.14.299.
[13] D.J. Chakrabarti, D.E. Laughlin, The Cu-S (Copper-Sulfur) system, J. Phase Equil. 4 (3) (1983) 254–271, https://doi.org/10.1007/BF02868665.
[14] E.H. Roseboom, An investigation of the system Cu-S and some natural copper sulfides between 25° and 700 °C//Econ, Geol. 61 (1966) 641–672.
[15] A. Guan, H. Wang, H. Jin, W. Chu, Y. Guo, G. Lu, An experimental apparatus for simultaneously measuring Seebeck coefficient and electrical resistivity from 100 K to 600 K, Rev. Sci. Instrum. 84 (2013) 043903, https://doi.org/10.1063/1.4798647.
[16] A. Janosi, La structure du sulfure cuivreux quadratique, Acta Crystallogr. 17 (1964) 311–312, https://doi.org/10.1107/S0365110X64000743.
[17] D. Byeon, R. Sobota, K. Delime-Codrin, S. Choi, K. Hirata, M. Adachi, M. Kiyama, T. Matsuura, Y. Yamamoto, M. Matsunami, T. Takeuchi, Discovery of colossal Seebeck effect in metallic Cu_2Se, Nat. Commun. 10 (2019) 72, https://doi.org/10.1038/s41467-018-07877-5.
[18] D. Byeon, R. Sobota, K. Hirata, S. Singh, S. Choi, M. Adachi, Y. Yamamoto, M. Matsunami, T. Takeuchi, Dynamical variation of carrier concentration and colossal Seebeck effect in Cu_2S low-temperature phase, J. Alloys Compd. 826 (2020) 154155, https://doi.org/10.1016/j.jallcom.2020.154155.
[19] M. Guan, P. Qiu, Q. Song, J. Yang, D.-D. Ren, X. Shi, L.-D. Chen, Improved electrical transport properties and optimized thermoelectric figure of merit in lithium-doped copper sulfides, Rare metals 37 (2018) 282–289, https://doi.org/10.1007/s12598-018-1007-0.
[20] H. Liu, X. Shi, F. Xu, L. Zhang, W. Zhang, L. Chen, Q. Li, C. Uher, T. Day, G.J. Snyder, Copper ion liquid-like thermoelectrics, Nature Mater 11 (2012) 422–425, https://doi.org/10.1038/nmat3273.
[21] W.-D. Liu, L. Yang, Z.-G. Chen, J. Zou, Promising and eco-friendly Cu_2X-based thermoelectric materials: progress and applications, Adv. Mater. 32 (2020) 1905703, https://doi.org/10.1002/adma.201905703.
[22] K. Zhao, P. Qiu, X. Shi, L. Chen, Recent advances in liquid-like thermoelectric materials, Adv. Funct. Mater. 30 (2020) 1903867, https://doi.org/10.1002/adfm.201903867.
[23] C. Coughlan, M. Ibáñez, O. Dobrozhan, A. Singh, A. Cabot, K.M. Ryan, Compound copper chalcogenide nanocrystals, Chem. Rev. 117 (2017) 5865–6109, https://doi.org/10.1021/acs.chemrev.6b00376.
[24] F.F. Jaldurgam, Z. Ahmad, F. Touati, Low-toxic, earth-abundant nanostructured materials for thermoelectric applications, Nanomaterials 11 (2021) 895, https://doi.org/10.3390/nano11040895.
[25] A. Basit, J. Xin, G. Murtaza, L. Wei, A. Hameed, W. Guoyu, J.Y. Dai, Recent advances, challenges, and perspective of copper-based liquid-like thermoelectric chalcogenides: a review, EcoMat 5 (2023) e12391, https://doi.org/10.1002/eom2.12391.
[26] W.-T. Yen, K.-K. Wang, H.-J. Wu, Hybridization of n-type Bi_2Te_3 crystals with liquid-like copper chalcogenide elicits record-high thermoelectric performance, Mat. Today Phys. 34 (2023) 101065, https://doi.org/10.1016/j.mtphys.2023.101065.
[27] H. Liu, J. Yang, X. Shi, S.A. Danilkin, D. Yu, C. Wang, W. Zhang, L. Chen, Reduction of thermal conductivity by low energy multi-Einstein optic modes, J. Materiomics. 2 (2) (2016) 187–195, https://doi.org/10.1016/j.jmat.2016.05.006.
[28] J. Gong, P.K. Jain, Room-temperature superionic-phase nanocrystals synthesized with a twinned lattice, Nat. Commun. 10 (2019) 3285, https://doi.org/10.1038/s41467-019-11229-2.
[29] Z. Zhu, ·Y. Zhang, ·H. Song, X.-J. Li, High thermoelectric performance and low thermal conductivity in $Cu_{2-x}Na_xSe$ bulk materials with micro-pores, Appl. Phys. A. 125 (2019) 572, https://doi.org/10.1007/s00339-019-2870-8.
[30] Y.-X. Zhang, J. Feng, Z.-H. Ge, Enhanced thermoelectric performance of $Cu_{1.8}S$ via lattice softening, Chem. Eng. J. 428 (2022) 131153, https://doi.org/10.1016/j.cej.2021.131153.
[31] J.-H. Li, Q. Tan, J.-F. Li, D.-W. Liu, F. Li, Z.-Y. Li, M.-M. Zou, K. Wang, BiSbTe- based nanocomposites with high ZT: the effect of SiC nanodispersion on thermoelectric properties, Adv. Func. Mater. 23 (2013) 4317–4323, https://doi.org/10.1002/adfm.201300146.
[32] P. Qin, Z.-H. Ge, Y.-X. Chen, X. Chong, J. Feng, J. He, Achieving high thermoelectric performance of $Cu_{1.8}S$ composites with WSe_2 nanoparticles, Nanotechnology 29 (2018) 345402, https://doi.org/10.1088/1361-6528/aac901.
[33] S. Zheng, S. Xiao, K. Peng, Y. Pan, X. Yang, X. Lu, G. Han, B. Zhang, Z. Zhou, G. Wang, X. Zhou, Symmetry-guaranteed high carrier mobility in quasi-2D thermoelectric semiconductors, Adv. Mater. 35 (2023) 2210380, https://doi.org/10.1002/adma.202210380.
[34] D. Zhang, X. Wang, H. Wu, Y. Huang, S. Zheng, B. Zhang, H. Fu, Z. Cheng, P. Jiang, G. Han, G. Wang, X. Zhou, X. Lu, High thermoelectric performance in earth-abundant Cu_3SbS_4 by promoting doping efficiency via rational vacancy design, Adv. Funct. Mater. 33 (2023) 2214163, https://doi.org/10.1002/adfm.202214163.
[35] G. Dennler, R. Chmielowski, S. Jacob, F. Capet, P. Roussel, S. Zastrow, K. Nielsch, I. Opahle, G.K.H. Madsen, Are binary copper sulfides/selenides really new and promising thermoelectric materials? Adv. Energy Mater. 4 (9) (2014) https://doi.org/10.1002/aenm.201301581.
[36] D.R. Brown, T. Day, T. Caillat, G.J. Snyder, Chemical stability of $(Ag,Cu)_2Se$: a historical overview, J. Electron. Mater. 42 (2013) 2014–2019, https://doi.org/10.1007/s11664-013-2506-2.
[37] D. Yang, X. Su, J. Li, H. Bai, S. Wang, Z. Li, H. Tang, K. Tang, T. Luo, Y. Yan, J. Wu, J. Yang, Q. Zhang, C. Uher, M.G. Kanatzidis, X. Tang, Blocking ion migration stabilizes the high thermoelectric performance in Cu_2Se composites, Adv. Mater. 32 (40) (2020) 2003730, https://doi.org/10.1002/adma.202003730.
[38] Z.-H. Ge, Y.-X. Zhang, T.-Y. Yang, D. He, Y. Xiao, H. Lai, Y. Wang, J. Deng, J.-F. Li, J. Feng, J. He, L.-D. Zhao, Highly stabilized thermoelectric performance in natural minerals, Joule 8 (2024) 129–140, https://doi.org/10.1016/j.joule.2023.11.013.
[39] P. Qiu, M.T. Agne, Y. Liu, Y. Zhu, H. Chen, T. Mao, J. Yang, W. Zhang, S.M. Haile, W.G. Zeier, J. Janek, C. Uher, X. Shi, L. Chen, G.J. Snyder, Suppression of atom motion and metal deposition in mixed ionic electronic conductors, Nat. Commun. 9 (2018) 1–8, https://doi.org/10.1038/s41467-018-05248-8.
[40] M.Kh Balapanov, A.F. Nadejzdina, R.A. Yakshibayev, D.R. Lukmanov, Ionic conductivity and chemical diffusion in $Li_xCu_{2-x}Se$ superionic alloys, Ionics 5 (1999) 20–22, https://doi.org/10.1007/BF02375898.
[41] S.D. Kang, J.H. Pohls, U. Aydemir, P.F. Qiu, C.C. Stoumpos, R. Hanus, M.A. White, X. Shi, L.D. Chen, M.G. Kanatzidis, G.J. Snyder, Enhanced stability and thermoelectric figure-of-merit in copper selenide by lithium doping, Mater Today Phys 1 (1) (2017) 7, https://doi.org/10.1016/j.mtphys.2017.04.002.
[42] E.M. Chen, P.F.P. Poudeu, Thermal and electrochemical behavior of $Cu_{4-x}Li_xS_2$ (x = 1, 2, 3) phases, J. Sol. St. Chem. 232 (2015) 8–13, https://doi.org/10.1016/j.jssc.2015.08.045.
[43] M.Kh Balapanov, R.A. Yakshibaev, I.G. Gafurov, R.Kh Ishembetov, ShM. Kagarmanov, Superionic conductivity and crystal structure of $Li_xCu_{2-x}S$ alloys, Bull. Russ. Acad. Sci.: Physics. 69 (2005) 623–626.
[44] R.D. Shannon, Revised effective ionic radii and systematic studies of interatomic distances in halides and chalcogenides, Acta Crystallogr. A32 (1976) 751–767, https://doi.org/10.1107/S0567739476001551.
[45] S. Åsbrink, L.-J. Norrby, A refinement of the crystal structure of copper(II) oxide with a discussion of some exceptional E.s.d.'s, Acta Cryst. B26 (1970) 8–15, https://doi.org/10.1107/S0567740870001838.
[46] S.C. Ray, Preparation of copper oxide thin film by the sol-gel-like dip technique and study of their structural and optical properties, Sol. Energy Mater. Sol. Cells 68 (2001) 307–312, https://doi.org/10.1016/S0927-0248(00)00364-0.
[47] A.V. Ushakov, I.V. Karpov, L.Yu Fedorov, E.A. Goncharova, M.V. Brungardt, V.G. Demin, Investigation of the effect of oxygen partial pressure on the phase composition of copper oxide nanoparticles by vacuum arc synthesis, Techn. Phys. 67 (15) (2022) 2410–2415, https://doi.org/10.21883/TP.2022.15.55268.157-21.
[48] B.K. Meyer, A. Polity, D. Reppin, M. Becker, P. Hering, P.J. Klar, T. Sander, C. Reindl, J. Benz, M. Eickhoff, C. Heiliger, M. Heinemann, J. Bläsing, A. Krost, S. Shokovets, C. Müller, C. Ronning, Binary copper oxide semiconductors: from materials towards devices, Phys. Stat. Sol. B. 249 (2012) 1487–1509, https://doi.org/10.1002/pssb.201248128.
[49] P. Von Kubaschewski, Spezifische Warmen und thermische Fehlordnung von Kupferchalkogeniden Teil II : Die Systeme Cu_2S - CuS und Cu_2Se – CuSe, Ber. Bunsen Ges. 2 (1973) 74–80, https://doi.org/10.1002/BBPC.19730770204.
[50] N. Yoshida, T. Naito, H. Fujishiro, Thermoelectric properties of Li-Doped CuO, Japan. Appl. Phys. 52 (2013) 031102, https://doi.org/10.7567/JJAP.52.031102.

[51] R.J. Cava, F. Reidinger, B.J. Wuensch, Mobile ion distribution and anharmonic thermal motion in fast ion conducting Cu_2S, Solid State Ionics 5 (1981) 501–504, https://doi.org/10.1016/0167-2738(81)90302-7.
[52] L.-W. Wang, High chalcocite Cu_2S: a solid-liquid hybrid phase, Phys. Rev. Letters 108 (2012) 085703, https://doi.org/10.1103/PhysRevLett.108.085703.
[53] A.V. Dmitriev, E.S. Tkacheva, Calculation of the thermoelectric characteristics of n- and p-type PbTe using a three-band electron spectrum, Moscow University Physics Bull 3 (2014) 38–44, https://doi.org/10.3103/S0027134914030072.
[54] Y. He, T. Day, T.S. Zhang, H.L. Liu, X. Shi, L.D. Chen, G.J. Snyder, High thermoelectric performance in non-toxic earth-abundant copper sulfide, Adv Mater 26 (2014) 3974–3978, https://doi.org/10.1002/adma.201400515.
[55] D.G. Cahill, S.K. Watson, R.O. Pohl, Lower limit to the thermal conductivity of disordered crystals, Phys. Rev. B 46 (1992) 6131–6140.
[56] L.P. Bulat, V.B. Osvenskii, A.A. Ivanov, A.I. Sorokin, D.A. Pshenay-Severin, V.T. Bublik, N.Y. Tabachkova, V.P. Panchenko, M.G. Lavrentev, Experimental and theoretical study of the thermoelectric properties of copper selenide, Semiconductors 51 (2017) 854–857, https://doi.org/10.1134/S1063782617070041.
[57] L.P. Bulat, A.A. Ivanov, B. Osvenskii V, D.A. Pshenay-Severin, A.I. Sorokin, Thermal conductivity of Cu_2Se taking into account the influence of mobile copper ions, Phys. Solid State 59 (2017) 2097–2102, https://doi.org/10.1134/S1063783417100080.
[58] S. Singh, S.K. Srivastav, A. Patel, R. Chatterjee, S.K. Pandey, Effect of nanostructure on thermoelectric properties of $La_{0.7}Sr_{0.3}MnO_3$ in 300–600 K temperature range, Mater. Res. Express 5 (2018) 055026, https://doi.org/10.1088/2053-1591/aac1e3.
[59] M. Balapanov, M. Kubenova, K. Kuterbekov, A. Kozlovskiy, S. Nurakov, R. Ishembetov, R. Yakshibaev, Phase analysis, thermal and thermoelectric properties of nanocrystalline $Na_{0.15}Cu_{1.85}S$, $Na_{0.17}Cu_{1.80}S$, $Na_{0.20}Cu_{1.77}S$ alloys, Eurasian J. Phys. Funct. Mater. 2 (2018) 231–241, https://doi.org/10.29317/ejpfm.2018020304.
[60] X. Wang, X. Xu, S.U.S. Choi, Thermal conductivity of nanoparticle–fluid mixture, J. Thermophys. Heat Trans. 13 (4) (1999) 474–480, https://doi.org/10.2514/2.6486.
[61] H. Lai, S. Singh, Y. Peng, K. Hirata, M. Ryu, R. Kevin, A. Ang, L. Miao, T. Takeuchi, Enhanced performance of monolithic chalcogenide thermoelectric modules for energy harvesting via Co-optimization of experiment and simulation, ACS Appl. Mater. Interfaces 14 (34) (2022) 38642–38650, https://doi.org/10.1021/acsami.2c06349.
[62] A.K.R. Ang, I. Yamazaki, K. Hirata, S. Singh, M. Matsunami, T. Takeuchi, Development of $Cu_2Se/Ag_2(S,Se)$-Based monolithic thermoelectric generators for low-grade waste heat energy harvesting, ACS Appl. Mater. Interfaces 15 (40) (2023) 46962–46970, https://doi.org/10.1021/acsami.3c09823.
[63] H.K. Lee, H. Jo, J.I. Lee, A.R. Koirala, H. Cho, W. Huh, M.S. Kang, Electrochemical lithium doping of $Cu_{2-x}S$ nanocrystal assemblies for tuning their near infrared absorbance, J. Mater. Chem. C 11 (2023) 4466–4473, https://doi.org/10.1039/d3tc00076a.
[64] R. Mulla, M.K. Rabinal, CuO/Cu_xS composites fabrication and their thermoelectric properties, Materials for Renewable and Sustainable Energy 10 (2021) 3, https://doi.org/10.1007/s40243-021-00189-7.
[65] M.H. Hebb, Electrical conductivity of silver sulfide, Chem. Phys. 20 (1952) 185–190, https://doi.org/10.1063/1.1700165.
[66] I. Iokota, On the electrical conductivity of cuprous sulfide: a diffusion theory, J. Phys. Soc. Jpn. 8 (5) (1953) 595–602, https://doi.org/10.1143/JPSJ.8.595.
[67] C. Wagner, The thermoelectric power of cells with ionic compounds involving ionic and electronic conduction, Prog. Solid Chem. Phys. 7 (1972) 1–37, https://doi.org/10.1016/0079-6786(72)90003-9.